



# Experimental study of micromilling process and deburring electropolishing process on FeCo-based soft magnetic alloys

Gabriel Villalba-Alumbreros<sup>1</sup> · Enrique Lopez-Camara<sup>1</sup> · Javier Martínez-Gómez<sup>1</sup> · Santiago Cobreces<sup>2</sup> · Ignacio Valiente-Blanco<sup>1</sup> · Efren Diez-Jimenez<sup>1</sup> 

Received: 5 December 2022 / Accepted: 17 March 2023 / Published online: 30 March 2023  
© The Author(s) 2023

## Abstract

FeCo-based soft magnetic alloys are commonly used in macroscale devices to improve its electromagnetic performance, whereas they have been barely used in the microscale. Current FeCo alloy micromanufacturing processes present some difficulties like low structural strength, oxidation at high temperature processes, stoichiometry mismatches in deposition processes and tough workability. In this work, a microcutting of FeCo-2 V-based soft magnetic alloys process is presented and described as an alternative method to obtain microparts with high magnetic properties and good geometrical finish. The results of the machining process are analysed by varying the machining parameters such as depth of cut, tool diameter, rotation speed and feed speed on simple machining operations. The study has been done for 50- $\mu\text{m}$ -diameter endmill and 250- $\mu\text{m}$ -diameter endmill tools. It concludes that the roughness is minimized when machining parameter combination is 0.24 mm/min of feed rate and 8  $\mu\text{m}$  of depth of cut size for a 250- $\mu\text{m}$ -diameter tool, while for a 50- $\mu\text{m}$ -diameter tool, the selected feed rate is 0.24 mm/min, for a depth of cut between 2 and 4  $\mu\text{m}$ . An automated precision 3-axis CNC station is used. Shapes needed for actuators such as angular slots, disks, or slender square geometries are shown in this work with excellent magnetic and mechanical properties. Additionally, a complementary electropolishing process is described. This process helps to eliminate burr in edges and residuals of the milling operation. This study demonstrates that micromilling can be a good alternative for microfabrication of FeCo-2 V components, suitable for precision microassemblies on MEMS.

**Keywords** Micromilling · Soft magnetic alloys · Surface roughness · Micromanufacturing · Microfabrication

## 1 Introduction

High-performance ferromagnetic materials are needed in plenty of unique magnetic components, which are required for several fields of application: electrical, electronical and mechanical engineering. In mechatronic devices with permanent magnets such as electric motors [1–3], actuators [4], generators [5, 6], robotic joints [7] and magnetic gears [8, 9], the use of ferromagnetic yokes on its construction implies a significative enhance of efficiency, torque and torque density. Miniaturization of these devices leads

to micro-electro-mechanical systems (MEMS). Micromotors [10], magnetic microgears [11, 12], sensors [13], wave absorbers [14], magnetic bearings [15–17] and microrobots [18] are some examples of MEMS technology which may include ferromagnetic parts.

Another field where its application is of particular interest is the manufacture of magnetic components for electrical and electronic systems— inductors and transformers — for its use in switching-mode power supplies for point-of-load applications [19], in computational systems for data centres or mobile devices. This system concept has been identified by the main manufacturers as an important line of development and business which are already considering Power-Supply-in-package or Power-Supply-on-Chip format as short-term ultimate goals [20, 21]. On this road to its miniaturization, the use of FeCo alloys is known to be an interesting option to be used as a material for the magnetic cores of these devices [22–24]. When compared to air-core alternatives, they offer a reduced switching frequency,

✉ Efren Diez-Jimenez  
efren.diez@uah.es

<sup>1</sup> Mechanical Engineering Area, Signal Theory and Communications Department, Universidad de Alcalá, 28801 Alcalá de Henares, Spain

<sup>2</sup> Electronics Department, Universidad de Alcalá, 28801 Alcalá de Henares, Spain

decreasing power semiconductors stress and losses; a lower number of coil turns, which implies a footprint reduction; and lower flux leaks between different windings of transformers reducing the need of snubber circuits and device voltage ratings [25–27].

High saturation magnetization ( $M_s$ ), high permeability ( $\mu$ ), low coercivity ( $H_c$ ) and high Curie temperature are characteristics of soft magnetic materials such as FeCo alloys [28, 29]. In general, FeCo alloys are brittle due to the formation of the ordered B2 phase [30]. Impacting, prohibitively poor ductility and low workability pose challenges to the conventional machining of these materials. Especially for small-size parts where the processing difficulty increases exponentially [31].

The creation of FeCo material with high quality, particularly in thin-film shapes, has always been a difficult achievement. This is due to its tendency of getting easily oxidized [32], also the effect of atomic diffusion of Co and Fe to the substrate [33]. Driving to the formation of complex oxides during the shaping of FeCo material, it complexifies the manufacturing of FeCo parts [34]. Techniques like excimer laser ablation process accomplish Tb<sub>0.4</sub>Fe<sub>0.6</sub>/Fe<sub>0.5</sub>Co<sub>0.5</sub> and Fe<sub>0.6</sub>Co<sub>0.4</sub>/SiO<sub>2</sub> multilayers of few microns of thickness in shapes of thousands of microns wide [35].

More complex structures applied in electronics and sensors such as nanowires and nanotubes of FeCo alloys have been achieved by anodic aluminium oxide template method of electrodeposition [36, 37]. The main pitfall is that these manufactured parts do not exhibit high levels of resistance against mechanical strain. Many electrical devices and structural components require higher aspect ratio bulk FeCo solid parts. Then, forming and machining of workpiece material processes are demanded to achieve the parts with the necessary mechanical integrity. Small-sized bulk FeCo parts have been successfully manufactured by micro-fast sintering at not high temperatures. The manufactured parts present a grain size of 5–6  $\mu\text{m}$  and a high level of densification during the process [30]. Other authors have achieved impressive results in electron beam-welded ultra-thin FeCo-V foils [38]. Another process to obtain high aspect features in soft magnetic composites is additive manufacturing process [39]. Alternatively, powder injection moulding has been developed aiming to create solid parts without vanadium addition to the composition, presenting also higher quality than traditional sintering parts [40]. However, the main drawbacks for all these methods are that the parts are not structurally consistent enough and that no micrometric features and complex shapes can be obtained.

Otherwise, there are cutting-edge technics in micromachining that enables complex 2D and 3D geometrical features by material removal for high magnetic quality FeCo workpiece material. Some of more precise

techniques are pulse laser ablation (PLA) [41], electrical discharge machining (EDM), focused ion beam (FIB) and chip removal micromachining processes. PLA offers precision machining in complex small 2D features and allows scalability of the machining process [42], although the possibilities of application depend on the surface finish and the optical properties of the material. In addition, the high temperatures reached during the process can damage the material magnetic properties. EDM offers different techniques (sink EDM, sink die EDM, wire EDM and hole drilling EDM), which allow very high aspect ratio parts [43] and complex 2D figures like microgears in hard materials [44], although it is restricted only to conductive materials. Through FIB manufacturing sharp geometries are possible, though a long machining time is required due to its very low machining rate.

In contrast, chip removal processes, in special micromilling, are cheaper, faster, simpler and one of the most reliable processes to obtain precise geometries, including straight walls and edges in most miniaturised products [45, 46]. Microcutting processes can be easily modelled and simulated, similarly to its macroscopic counterpart processes. In submillimetre scale cutting tools, the physical behaviour of cutting is still invariant with respect to the macroscopic size. Scaling conventional machining methods in microcutting techniques allows achieving geometrical features with characteristic length from few millimetres to tens of microns [47]. This is because micromilling cutters have well-defined cutting edges that can achieve high machined surface integrity and dimensional/geometrical accuracy, complex machining contours and challenging structures [48–50].

The physical mechanisms of chip cutting, formation and removal from the workpiece material have inherent problems in the microscale not present in the macro scale [51–53]. This affects milling results and possibilities. There are many parameters related to the accuracy and finish on the process such as tool and material hardness, size effect, tool diameter, chip thickness, feed and cutting velocities and process stability [46]. Therefore, it is important to thoroughly analyse the main physical processes that limit the efficiency and precision of the process in micro-milling. There are experimental works in literature about micromilling in hard materials such as stainless steel or titanium alloys [54]. Nevertheless, as far as we are concerned, there is no previous work on studying micromilling fabrication possibilities in FeCo soft magnetic alloys.

In this work, a systematic experimental study on micromilling processes on Fe–Co–V-based soft magnetic alloys is presented. Input (feed rate, rotational speed, depth of cut) and output results (surface roughness, groove depth, groove width) are described and analysed from the results. In addition, application examples are presented with complex

geometries including submillimetric parts with micrometric features made in FeCo soft magnetic alloy.

## 2 Materials and methods

### 2.1 Micromilling workstation

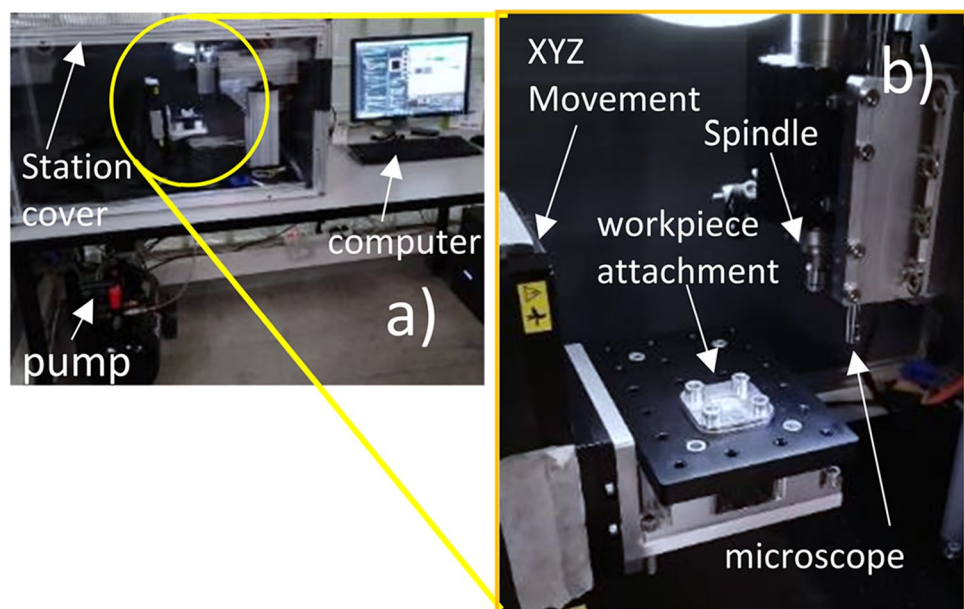
The micro-milling process was conducted on a precision three-axes machine tool. This machining tool is a computer numerical control (CNC) workstation specifically developed and customized for the microscale (Fig. 1). It can obtain drilling and milling of micrometric features. This machine can perform 3D XYZ movements with submicrometre precision. This CNC station can mill and drill using micrometric cutting tools. It also includes a USB microscope that allows recalibration and referencing procedure using visual feedback from the microscope which is installed on the machine in parallel to the spindle. The design of the micromilling machine tool is oriented to produce small structures. The station basically includes XYZ motion tables and a rigidly fixed spindle head (Fig. 1). Micro-milling CNC has three ultraprecision linear motor stages with built-in controllers and linear encoders provided by Zaber Technologies INC company. XY axes are moved by means of model X-LDM110C-AE54D12 (intended for horizontal displacements) and X-LRQ075AP-DE51C for the Z-axis of the station. XY tables have a travel of 110 mm with a positioning accuracy below 1  $\mu\text{m}$ . Due to this small size, small axes with low travel and low moving masses could be implemented, resulting in high velocities and low energy consumption. The attachment of the workpiece material laminates is done by using a vacuum chuck. This permits to

flatten the laminate and assure the parallelism. The spindle is a Sycotec 4033 AC-ER8 model of 420 W of power, with a maximum rotational speed of 100,000 rpm, a maximum torque of 8.4 Ncm and a run-out of 1  $\mu\text{m}$  at a selected speed of 30,000 rpm. The spindle, as well as the spindle mount, is air-cooled. Microparticles and nanoparticles are removed by pressurized air. The micromilling station is protected by a transparent casing with which it is possible to carry out all the micro-milling and prevent dust contamination. The whole micro-milling tool is desktop-sized covering a total volume of 900 mm  $\times$  600 mm  $\times$  500 mm.

### 2.2 FeCo material and micromilling tool

FeCo alloys are generally little ductile and hard to work. To enhance its machinability and stiffness, vanadium additive is included in the composition. With this additive, the magnetic performance is slightly decayed, the magnetic permeability is decreased, and the coercivity increases [55]. In the case of FeCo–2 V alloys, this decay can be down to 10% regarding the equiatomic FeCo [56], depending on the heat treatment. Three commercial FeCo–2 V alloys have been chosen: Vacodur49, Vacoflux48 and Hiperco50 depending on the laminate thickness. These three materials present a composition of 49% cobalt, 49% iron and 2% vanadium. These materials present the highest magnetic saturation and greater mechanical strength than other soft magnetic alloys. Selected FeCo–2 V alloys are purchased in cold rolled laminated, with thickness between 55 and 355  $\mu\text{m}$ . They exhibit yield strength of 1150–1270 MPa, tensile strength of 1230–1310 MPa, a typical Poisson's ratio of 0.29, Young's modulus of 200–206 GPa, hardness between 342 and 380

**Fig. 1** Micromilling CNC workstation (a) and mechanical elements (b)



HV, density of  $8.12 \text{ g/cm}^3$  and expansion coefficient  $8.9\text{--}9.7$  (20 to  $200 \text{ }^\circ\text{C}$ )  $\alpha [10^{-6}/\text{K}]$ .

Micro-milling was performed by MF208-0005-0008-M with  $50\text{-}\mu\text{m}$ -diameter and MF208-0025-0038-M with  $250\text{-}\mu\text{m}$ -diameter end mills pro metal, 2-flute stub with an helix angle of  $28^\circ$ , fishtail and stub end-mill from company FrezyCNC Ingraph (Poland). The tool diameters selected are  $50 \mu\text{m}$  as the minimum available and  $250 \mu\text{m}$  the maximum that allows machining features below  $100 \mu\text{m}$ . The tool material is solid submicrograin carbide. This material has a typical hardness of  $1350\text{--}1600 \text{ HV}$ , a transverse rupture strength of  $3100\text{--}3650 \text{ MPa}$  and a density of  $14\text{--}14.5 \text{ g/m}^3$ . These tools were chosen because cutting-edge geometry virtually eliminates chatter at high feed rates. Spiral geometry ensures efficient debris removal, and flute geometry enhances rigidity for accurate, single-pass cutting at high chip loads. Furthermore, the material selected for tools is suitable to cut FeCo-2 V. The used tools are shown in Fig. 2.

### 2.3 Material preparation and machining process

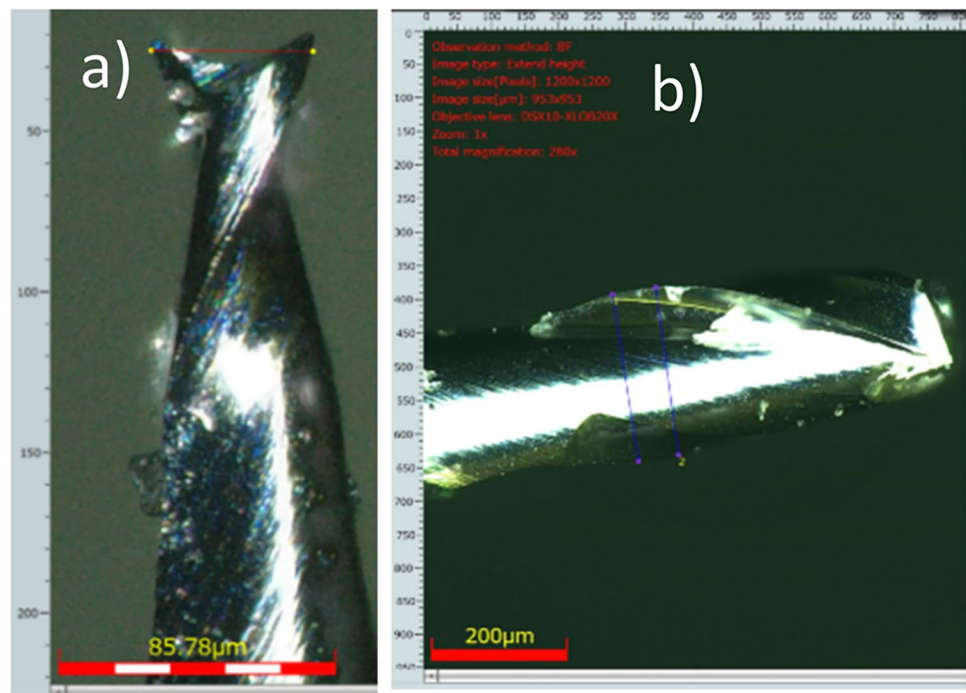
There are several steps to execute before the milling process action. The spindle motor must be warmed-up before the first machining. Then, tool and material are manually attached to the CNC station. The preparation of the material is the most delicate step before milling. Flatness and tilting errors may appear during the attachment of the laminate if it is not carefully executed. This results in geometrical and finishing defects on the final machined

part. After the laminate cutting, the workpiece material is flattened in a hydraulic press. The laminate is glued to a PVC substrate; this contributes to the rigidity of the laminate during machining. This attachment permits the milling of the ulterior release of the machined microparts. The complete attachment system is shown in Fig. 3. It includes two stainless steel case parts that press and fixes the laminate by using four screws tightening.

Once the material and tool are correctly positioned, it is necessary to visual reference using the microscope to locate the place where to start the machining. This defines XY (horizontal) zero position. Furthermore, the zeroing in Z axis is also needed when changing tool or material thickness. It is done by electric contact between the tooltip and the workpiece material.

The design is programmed on CAD-CAM software, where machining processes can be translated to a G-CODE program which is read by the software of the machine. Spindle rotation velocity, feed rate, tool diameter, bulk material thickness, depth of each step and geometry are specified on the CAD-CAM software. After all the preparation steps are achieved, the machining process can start. The machining is done under a big drop of lubricant coolant to improve heat dissipation and the process of chip cutting. Finally, the workpiece material is removed and immersed in a soft solvent like acetone to eliminate the adhesive layer, separating the machined metallic plate or the micropart from the PVC glued substrate.

**Fig. 2** Solid carbide micromills of  $50 \mu\text{m}$  (a) and  $250 \mu\text{m}$  (b) of diameter



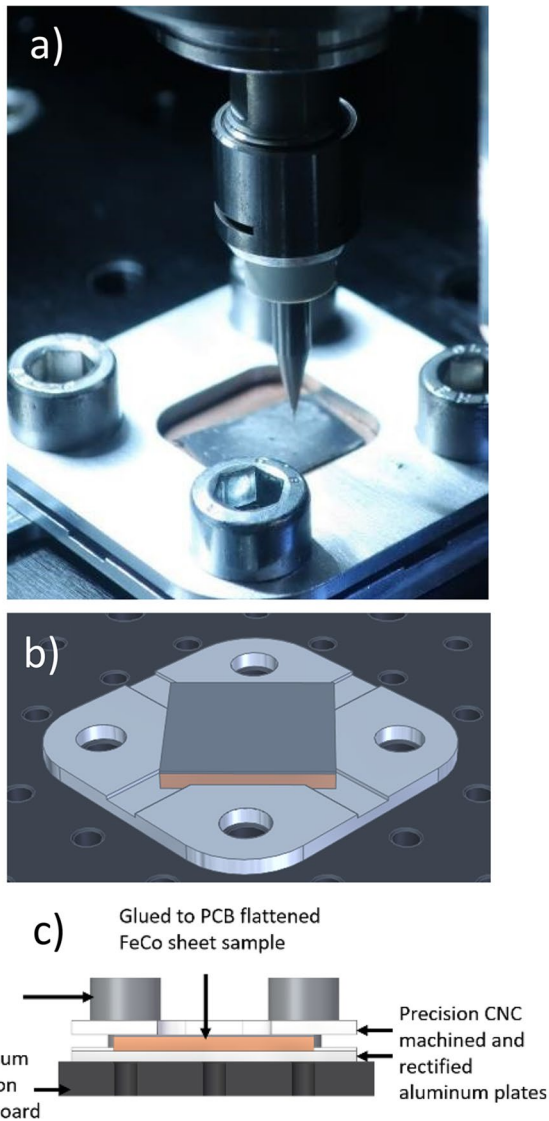


**Fig. 3** Attached workpiece material (a), bottom fixing part and workpiece material (b), attachment system elements in cut view (c)

**Table 1** Machining parameters considered in the study

Tool diameter, $D$ , ( $\mu\text{m}$ )	50 and 250
Spindle rotation speed, $n$ , $\text{min}^{-1}$	30,000 and 60,000
Feed rate, $f$ , $\text{mm}/\text{min}$	0.24, 0.48 and 0.96
Depth of cut, $p$ , $\mu\text{m}$	2, 4, 8 and 16

## 2.4 Experimental study test description

The micromilling systematic study includes different machining parameter values. The variation of the different parameters is listed in Table 1. The study is done by milling simple 1-mm straight grooves with single step and depth values to determine the optimal combination of machining

parameters. The range of parameters such as feed or depth step have been selected after selecting the best trial-and-error results based on visual inspection and burr measurements. The reasons of sweeping these parameters are, mainly, to achieve values that allow minimum burr formation and minimum geometrical deviation (due to plasticization effects in work material). The selected speed of 30,000 rpm corresponds to the minimum amplitude of vibration measured in the XY plane of the spindle structure through accelerometers, although the speed of 60,000 rpm is also studied to test the effect of those vibrations.

The analysis of the milling results is done using an Olympus DSX1000 digital microscope that allows two-dimensional and three-dimensional (2D and 3D) measurements. This microscope is connected to a computer located next to the cabin to check the results. The microscope enables fast macro to microlevel view, and it also provides accurate measurements due to its telecentric optical system. This microscope provides information about the geometric and surface roughness values of the manufacturing results.

## 3 Micromilling results and discussions

### 3.1 Geometric characterization

Once the 1-mm grooves are done at each different combination, measurements of resulting depth and width were done by profilometer, and geometric measurements were done by the confocal digital microscope. Several measurements were taken along each groove obtaining mean values and typical deviations for depth and width. For width measurements, a typical deviation is less than  $2\ \mu\text{m}$  for each groove, while it is less than  $0.6\ \mu\text{m}$  for depth of cut measurements. The excess of expected dimension is plotted in Fig. 4, for width, and in Fig. 5, for depth. The excess in width is calculated in respect to the tool diameter and the excess in depth of cut is the difference in  $\mu\text{m}$  with the programmed depth of cut in the G code program. Feed rate ( $f$ ), tool diameter ( $D$ ) and depth of cut ( $p$ ) are considered. The rotation spindle speed is set up as  $n=30,000\ \text{rpm}$  for all the geometrical characterization experiments. The excess of width is assumed to come from small eccentricity of the spindle and from non-controlled vibrations. Excess of width is reduced; thus, we consider that feed speed and microcutting forces are adequate.

Regarding cut width, the feed rate of  $0.48\ \text{mm}/\text{min}$  presents the smaller deviations for all diameters and depth of cuts, it is particularly critical for the  $50\text{-}\mu\text{m}$ -diameter tool at  $4\text{-}\mu\text{m}$  depth of cut. It is visible that the excess in width is not much dependent on the feed for the  $250\text{-}\mu\text{m}$  diameter tool in the range observed. It seems to be a depth threshold from where the width excess increases and becomes more dependent on the feed velocity. The set of parameters that more

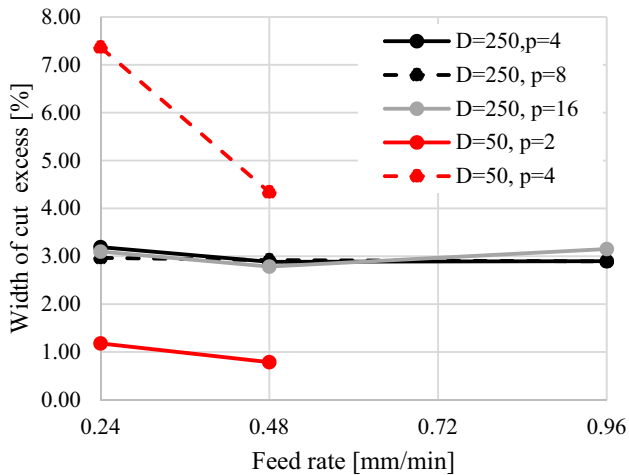


**Fig. 4** Groove width excess vs feed rate for various depths of cut ( $p$ ) and tool diameter ( $D$ )

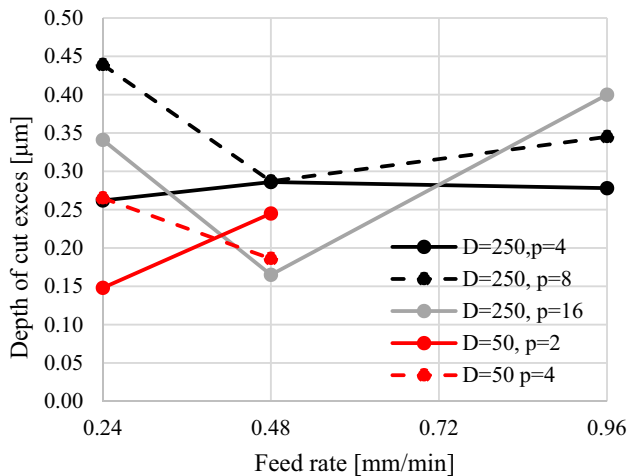
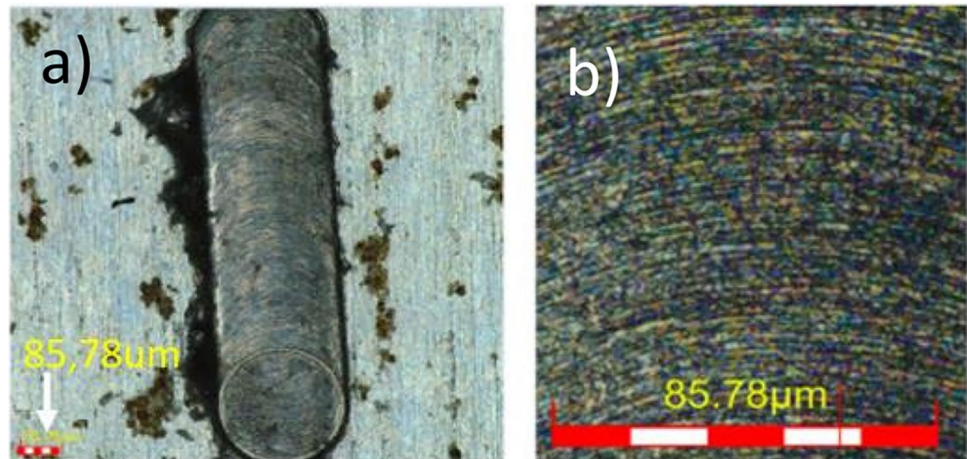


**Fig. 5** Groove depth excess vs feed rate for various depths of cut ( $p$ ) and tool diameter ( $D$ )

**Fig. 6** Microscope pictures of 250- $\mu$ m grooves (**a**) and its machined surface (**b**) at 0.48 mm/min feed, with  $p=16 \mu$ m, in **a** and **b**



accuracy offers in 2D geometrical features is the 50- $\mu$ m diameter tool at depth of cuts as small as 2  $\mu$ m, and machining at feed velocity of 0.48 mm/min, with width excess less than 1% of the diameter.

Regarding depth of cut, small deviations on the depth of grooves have been obtained, and the measured values vary between 0.15 and 0.45  $\mu$ m. The minimum value achieved for the 50- $\mu$ m diameter tool has been found at 2  $\mu$ m and 0.24, while for the 250  $\mu$ m diameter tool, it is found that at 16- $\mu$ m depth and 0.48. There is not a clear sign on influence neither tool, depth of cut, nor feed rate. They all seem to be adequately selected. We assume this variation comes from variation in the spindle tool position and from the zero-tooling process.

Figures 6 and 7 show pictures of the machining achieved by the two tools on their optimal parameter configurations, respectively. Straight walls, flat machined surface, fine width accuracy, and a small amount of burr have been achieved in this milling process. This is the starting point for more complex 2D features in multiple depth of cuts milling processes.

### 3.2 Roughness characterization

Roughness is calculated by the microscope Olympus software; several parameters of roughness can be measured being the most representative Ra which is defined as Average or arithmetic average of profile height deviations from the mean line. Ra measurements of the studied grooves have been taken. In addition, the effect of runout at not-optimal spindle velocities for the machine on the machined surface roughness has been studied.

Figure 8 shows that for all cases, smaller depth of cut means a lower roughness level. The effect of feed rate increases drastically when increasing the size of the depth of cut. Ra does not show a relevant dependency on tool diameter in the range of 50–250  $\mu$ m if the depth of cut

**Fig. 7** Microscope pictures of 50- $\mu\text{m}$  grooves (a) and its machined surface (b) at 0.48 mm/min feed, with  $p=2\ \mu\text{m}$ , in a and b

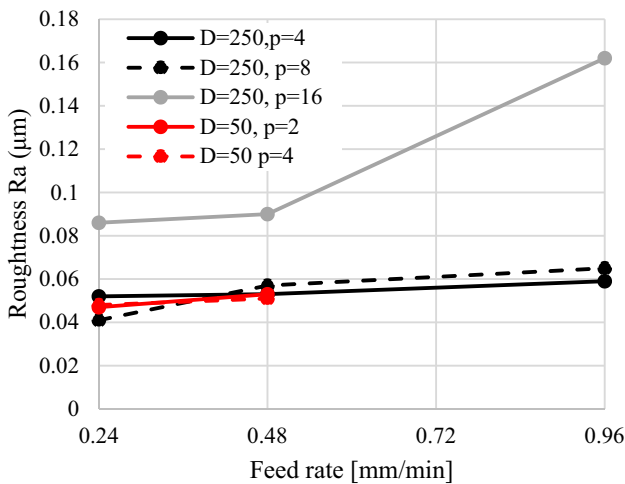
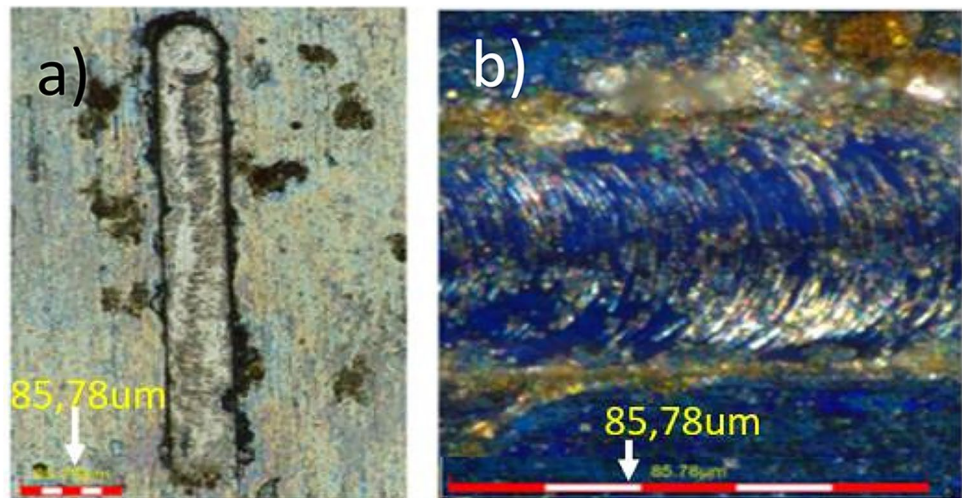


**Fig. 8** Ra roughness vs feed rate for various depths of cut ( $p$ ) and tool diameters ( $D$ )

is less than 8  $\mu\text{m}$  and the feed rate is between 0.24 and 0.48 mm/min. With both tools, the roughness achievable is small enough to satisfy the mechanical requirements on complex MEMS assemblies. Figure 9 shows a topographical view of the machined surface of the minimum roughness achieved with the 50- $\mu\text{m}$  tool; the  $S_a$  value of the marked area is 0.042, which is consistent with the Ra value shown in Fig. 5. Figure 10 shows the surface finish of the machined surface with the minimum roughness achieved of  $R_a=0.04\ \mu\text{m}$ . These values of roughness are small enough to achieve the required airgap thickness in microactuators such as micromotors, where airgaps around 10  $\mu\text{m}$  are needed.

The vibration of the tool leads to worse surface finishes and worse geometrical accuracy as shown in Fig. 11. In

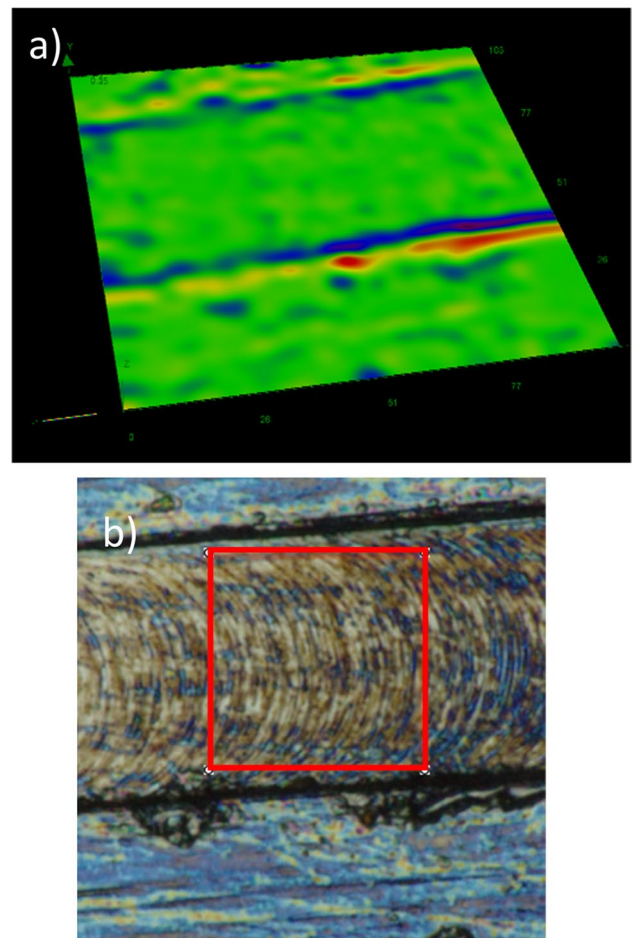


**Fig. 9** Topographical image of the roughness surface in a 50- $\mu\text{m}$  width groove (a), and the region used to measure  $S_a$  (b). Purple corresponds to 0  $\mu\text{m}$ , and red corresponds to 0.5  $\mu\text{m}$

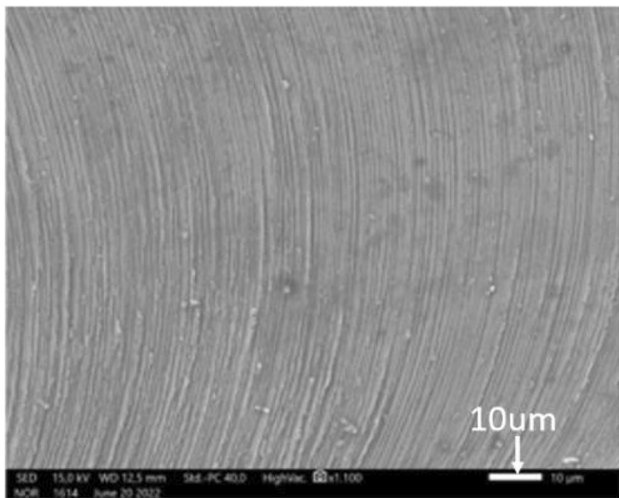


**Fig. 10** SEM image of FeCo2V machined surface with a 250- $\mu$ m diameter milling tool at 0.24 mm/min and 8  $\mu$ m of depth of cut size

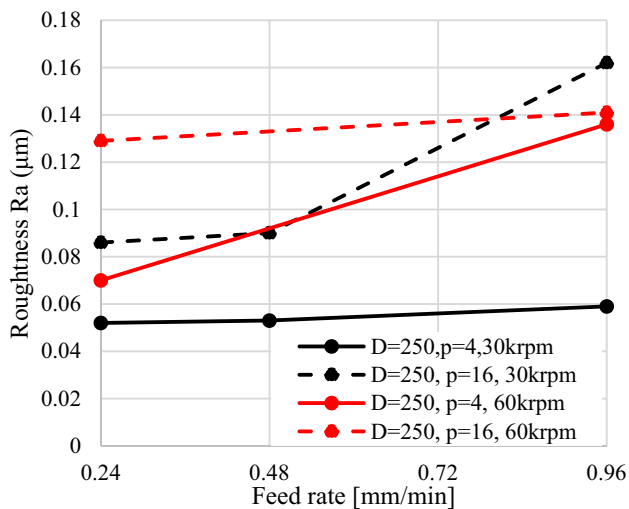


**Fig. 11** Ra roughness vs feed rate for various depths of cut ( $p$ ) and spindle rotation velocity ( $n$ ) for 250- $\mu$ m diameter tool

**Fig. 12** Microscope pictures of groove (a) and its machined surface (b) done at 0.24 mm/min feed rate, 16  $\mu$ m depth of cut size at 60 krpm, a 250- $\mu$ m diameter milling tool

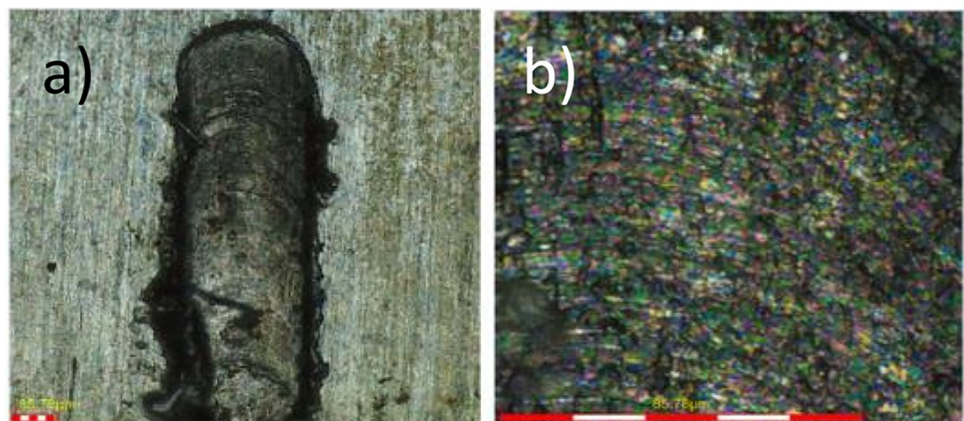


Fig. 12, it is visible a poorer finish and a worse geometrical shape in comparison to the milling shown in Fig. 6.

### 3.3 Application cases

For most electric machine applications, individual magnets are mounted in the rotor assembly. Rectangular plates, in radial flux applications, and circular sectors or segments, in axial flux applications, are the typical shapes needed for this kind of machines. One example of these desired shapes is the angular sector performed in FeCo-2 V alloy shown in Fig. 13. Adjusting the machining parameters to the optimized values for the 50-micron endmill, the shape has been performed in several cutting steps to achieve the desired depth of 50  $\mu$ m. The machined cavity presents high-quality straight walls and a very reduced quantity of burr in the top edges; this is visible in the vertical slice profile plotted in Fig. 13 bottom. This microscope provides information about the geometric and surface roughness values of the manufacturing results.

This kind of geometry can be radially duplicated, as the machined yoke of rotor in Fig. 14, creating ferromagnetic structures where assembling and gluing separated micromagnets is possible. In addition, there is the possibility of cutting out the part by milling, after integrating permanent magnets. The repeatability of this and more complex features is quite stable. In the machined patron of Fig. 14, the grooves were done by a 100- $\mu$ m milling tool. The width of the machined groove exceeds an average of 12.9  $\mu$ m, with a typical deviation of 2.18  $\mu$ m. The diameter of tool entrance presents an average excess of 11.5  $\mu$ m with a typical deviation of 3.83  $\mu$ m.

Figure 15 shows another example of a micropart made in FeCo-2 V alloy. The circular micropart has been cut out. It can be used as back yoke in stator or rotor assemblies of axial flux micromotors. The micropart is glued to a PVC substrate while it is being machined. Afterwards, the substrate with glued FeCo-2 V alloy laminate and



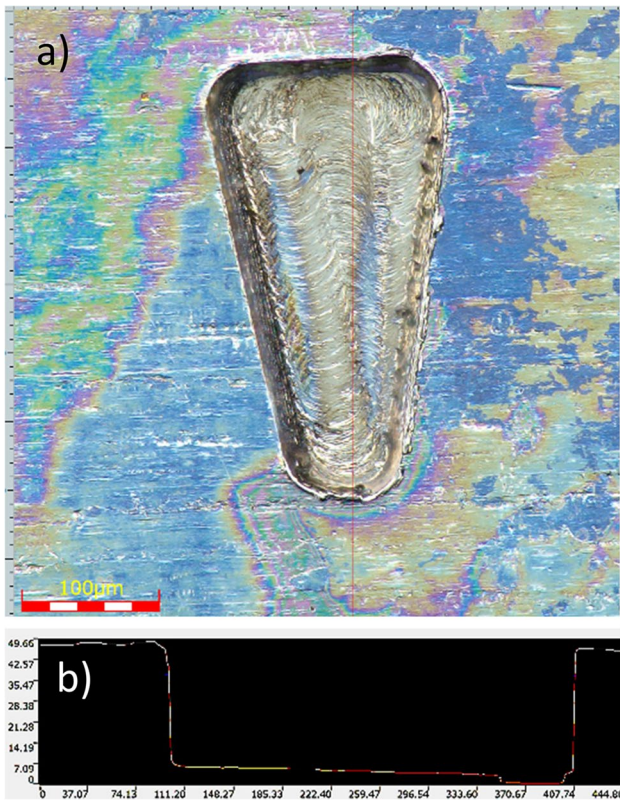


**Fig. 13** Angular sector shaped machined in Vacodur49 with a 50-µm diameter tool (a) and profile along red line (b)

machined part is submerged in acetone. The glue is dissolved, and the part is released without residuals.

Other interesting shapes are solenoid, stator and transformer yokes. This consists of high aspect ratio components with circular or square section shapes. These components are wound with aluminium, silver or copper wires. When an electrical current flows through the conductor, the ferromagnetic yoke becomes an electromagnet.

Some trials have been performed on FeCo-2 V; Fig. 16 shows square yokes of 150 × 150-µm size and 60-µm depth. It is visible the good quality of machined surfaces and the straightness of the walls. It presents a slight amount of burr and chip material on the upper edges. More complex yoke shapes have been achieved such as the one shown in Fig. 17. It is a near square yoke of 100-µm diameter and 200-µm height, over a circular base of 300-µm diameter and 100-µm height. This kind of slender geometries is required as yokes to be wound, wound yokes, are active electromagnetic components needed in devices such as actuators.

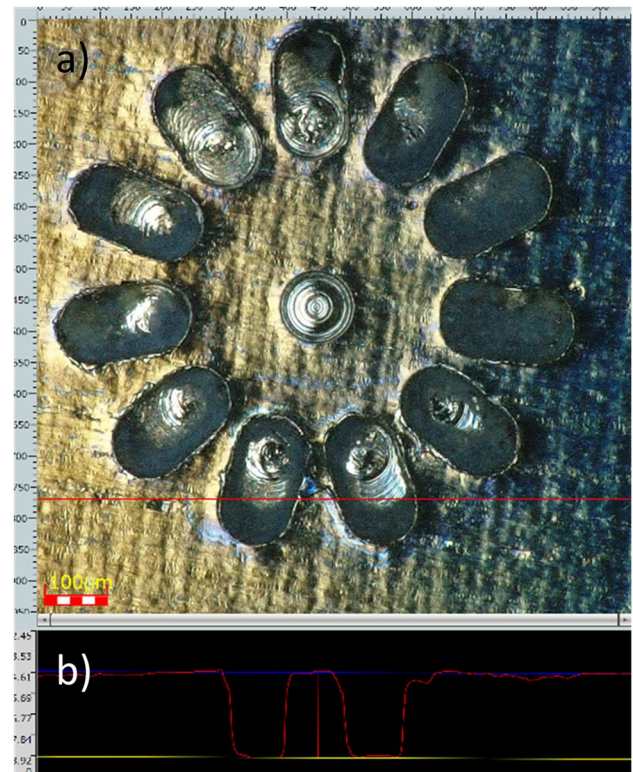


**Fig. 14** Machined rotor back yoke on FeCo-2 V alloy (a) and profile along the red line (b)

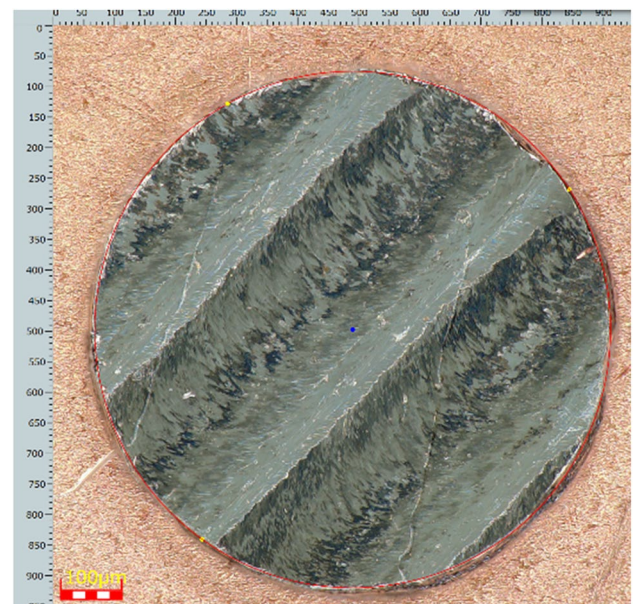


**Fig. 15** Micropart machined 0.9-mm diameter disk

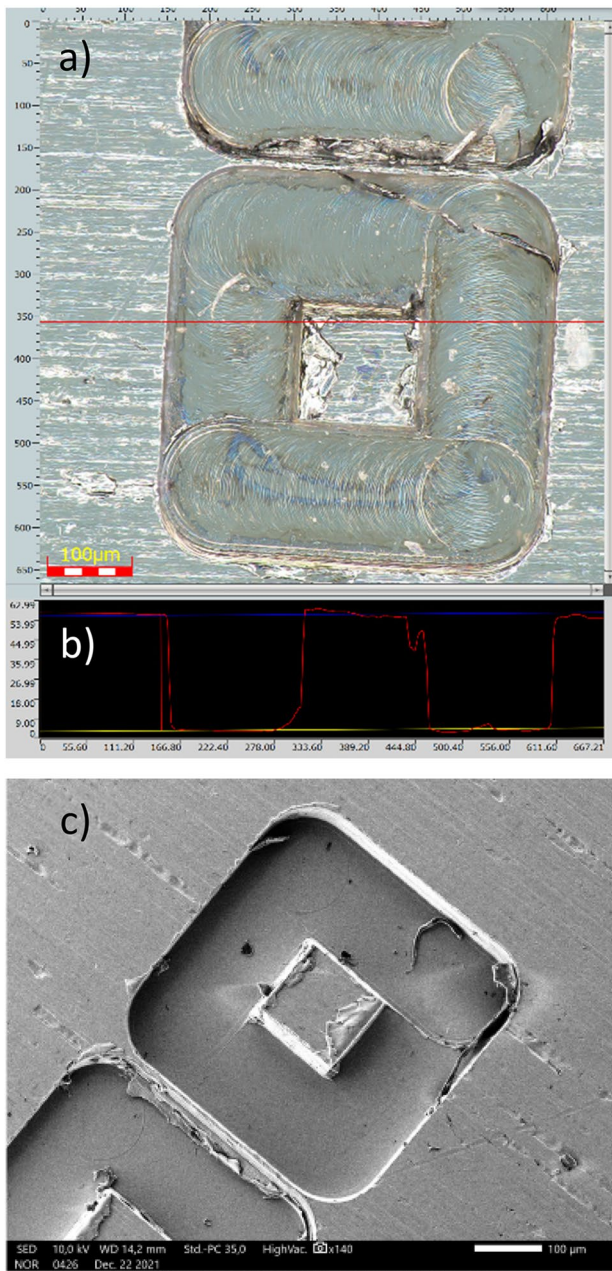


**Fig. 16** Square yoke machining trials; optical microscope capture (a), profile along the red line (b), SEM capture (c)

### 3.4 Deburring and cleaning process by electropolishing

Even though machining parameters have been selected to minimize machining imperfections, it is not possible to fully machine without any burr residuals. This defect may affect to the assembly process of micrometric components. An electrochemical process is applied to the machined parts to eliminate the burr imperfection on edges as a complementary process.

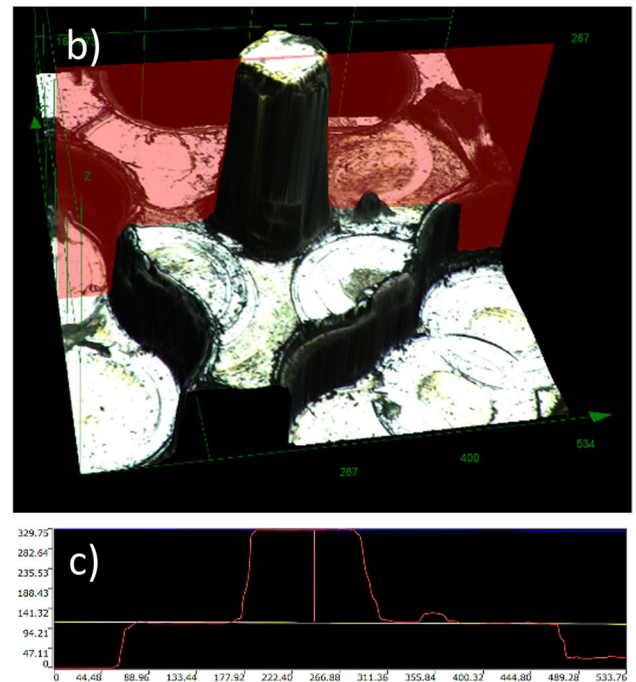
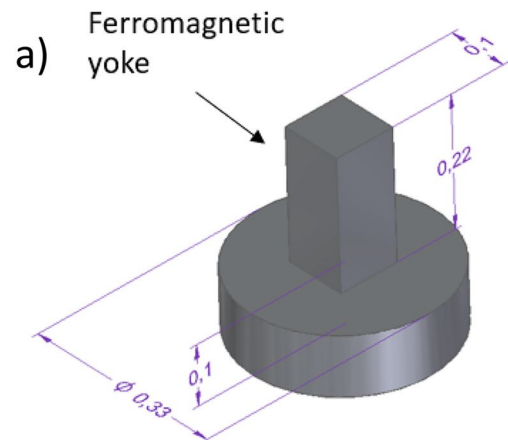


**Fig. 17** Ferromagnetic yoke design for electromagnet (a), machined yoke with base (b) and profile along the red plane (c)

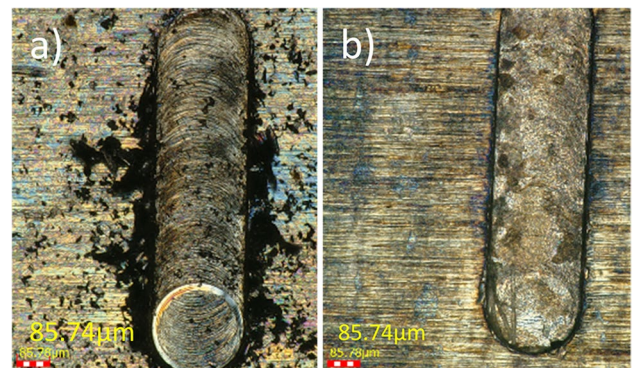


**Fig. 18** A 250- $\mu\text{m}$  width, 30- $\mu\text{m}$  depth groove after machining (a) and after being electropolished (b)

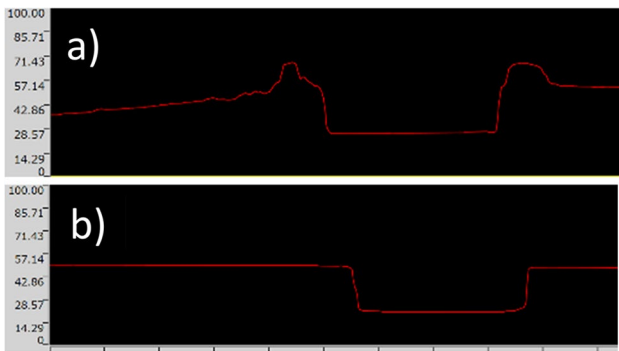


**Fig. 19** Comparison between section profile before (a) and after (b) electropolishing process in the 250- $\mu\text{m}$  width, 30- $\mu\text{m}$  depth groove

To achieve a better surface finish, electropolishing is done in an acid bath. The power supply is set to 0.7–0.8 V, a resistance of 0.4, 0.5  $\Omega$  appears, the total time needed is between 90 and 135 s to remove impurities and burrs, the positive cathode is hooked to the workpiece material from which the material must be removed (FeCo-2 V alloy) and the negative to the recipient, which is copper. The solution is 50% water and 50% hydrochloric acid of 10% of purity in volume. In Fig. 18 a groove of 250- $\mu\text{m}$  width and 30- $\mu\text{m}$  depth is shown before and after the electropolishing process. A 14- $\mu\text{m}$  bulge of burr and uncut chip gets completely eroded after electropolishing, as Fig. 19. The difference in finishing is key to make a machined part suitable to assembly in MEMS. This process solves one of the most important drawbacks of microcutting processes.

The machined rotor on FeCo-2 V shown in Fig. 14 is used as a practical example of the effectiveness of the electropolishing process. Considering the power applied and the submerged surface of FeCo-2 V workpiece material, the current density applied is about 320  $\text{A}/\text{m}^2$ .

Figure 20 shows the micropart after the polishing process, and Fig. 21 shows the comparison between section profiles before and after polishing. It is clearly visible that the process allows eliminating the burr residuals and surface irregularities without damaging the machined shape.

## 4 Conclusions

Plenty of cutting-edge micrometric applications on MEMS such as submillimetre motors, robots, sensors, magnetic gears and power converters require ferromagnetic components. These micro applications could be enhanced by using highly performant soft magnetic alloys like FeCo-based ones. However, the current FeCo alloy micromanufacturing process presents some difficulties like low structural strength, oxidation at high temperature processes, stoichiometry mismatches in deposition processes

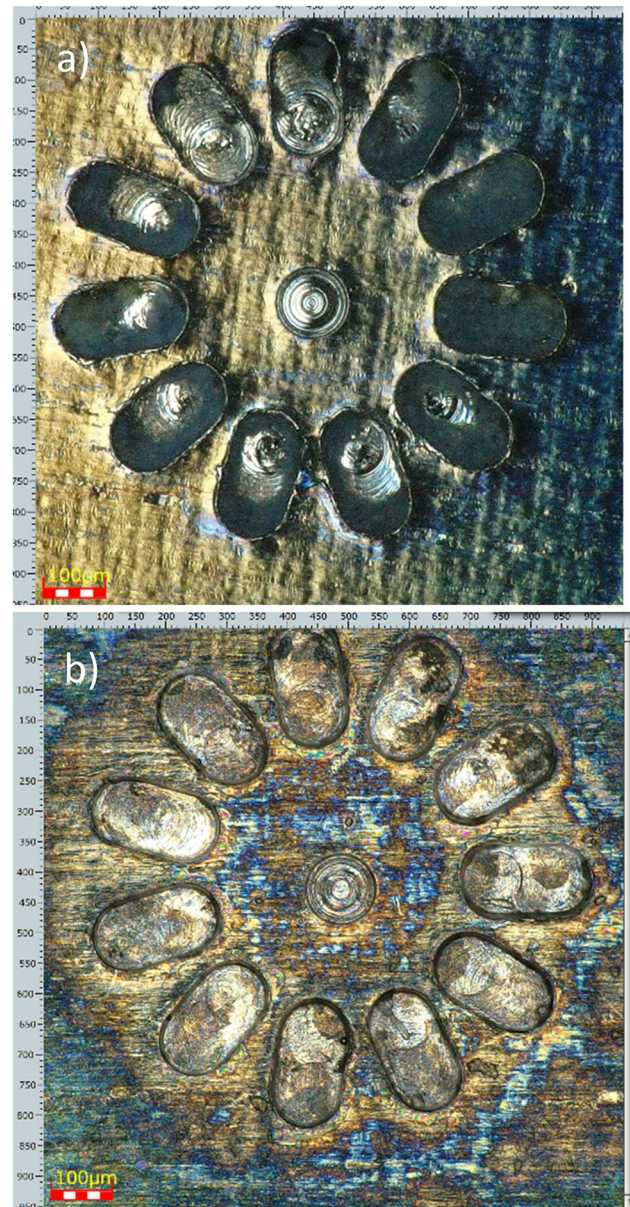
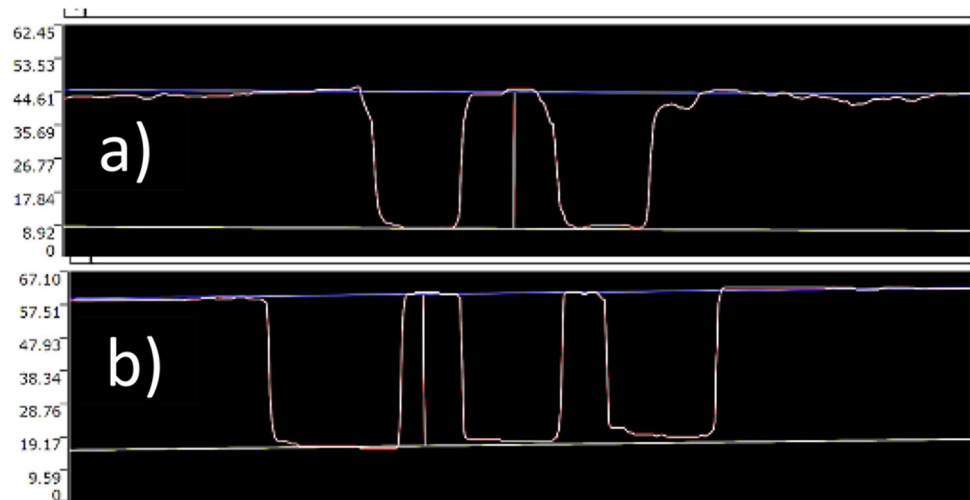


**Fig. 20** Electropolished machined embedded rotor back yoke before (a) and after (b)

and tough workability. Micromilling, then, is presented as an alternative method to achieve FeCo-based microparts maintaining the macroscopic bulk material properties with precision and geometrical 3D micrometric features. In this work, an experimental study of micromilling process on FeCo-based soft magnetic alloy is presented.

Different FeCo-2 V commercial soft magnetic alloys have been selected for micromilling trials. A systematic study of micromilling results has been done for 50- $\mu\text{m}$  diameter endmill and 250- $\mu\text{m}$  diameter endmill tools. The study demonstrates that micromilling is a good alternative for microfabrication of FeCo-2 V components. It concludes

**Fig. 21** Comparison between section profile before (a) and after (b) electropolishing process in the embedded rotor back yoke



that the roughness is optimized when machining parameter combination is 0.24 mm/min of feed rate and 8  $\mu\text{m}$  of depth of cut size for a 250- $\mu\text{m}$  diameter tool, while for a 50- $\mu\text{m}$  diameter tool, the optimal feed rate is 0.24 mm/min, for a depth of cut between 2 and 4  $\mu\text{m}$ . The optimal spindle rotation speed is found at 30,000 rpm, while other velocities like 60,000 rpm can make the roughness increase more than two times. The excess groove width remains about 3% for the 250- $\mu\text{m}$  diameter tool, and the value is stable in the ranges of 0.24–0.96 mm/min of feed and 4–6  $\mu\text{m}$  of depth of cut. For the 50- $\mu\text{m}$  tool, the minimum value of width excess is 0.8%, and it is reached at 0.48 mm/min of feed and 2  $\mu\text{m}$  of depth of cut size. The deviation in depth varies from 0.15 to 0.45  $\mu\text{m}$  in the experiments done. All results show that micromilling FeCo2V alloys with very small deviations and imperfections are possible.

As demonstrators, complex microparts have been machined in multiple milling steps: angular sectors, rotors, square and circular cylinders and 3D yoke geometries. Separated micromachined microparts have been achieved. For a better surface and edge finish, the electropolishing process has shown a complete reduction of burr in machined edges without altering the machined geometry. This study opens new possibilities on MEMS manufacturing using high magnetic performance precision microparts with excellent magnetic and mechanical properties.

**Author contribution** Gabriel Villalba-Alumberos: writing—review and editing, methodology, investigation. Enrique Lopez-Camara: resources, software. Javier Martinez-Gomez: investigation, writing—original draft. Santiago Cobrecas: investigation, conceptualization, writing. Ignacio Valiente-Blanco: validation, resources. Efren Diez-Jimenez: validation, methodology.

**Funding** Open Access funding provided thanks to the CRUE-CSIC agreement with Springer Nature. This research was supported by the European Union's Horizon 2020 research and innovation programme

under grant agreement No 857654–UWIPOM2. In addition, this work was partially supported by the Spanish Ministry of Science, Innovation and Universities under Ramón & Cajal Research Grant number RYC-2017–23684.

## Declarations

**Conflict of interest** The authors declare no competing interests.

**Open Access** This article is licensed under a Creative Commons Attribution 4.0 International License, which permits use, sharing, adaptation, distribution and reproduction in any medium or format, as long as you give appropriate credit to the original author(s) and the source, provide a link to the Creative Commons licence, and indicate if changes were made. The images or other third party material in this article are included in the article's Creative Commons licence, unless indicated otherwise in a credit line to the material. If material is not included in the article's Creative Commons licence and your intended use is not permitted by statutory regulation or exceeds the permitted use, you will need to obtain permission directly from the copyright holder. To view a copy of this licence, visit <http://creativecommons.org/licenses/by/4.0/>.

## References

- Kondelaji MAJ, Tazehkand MZ, Farahani EF, Mirsalim M, Khorsandi A (2020) A preliminary study on flux-boosted enhanced-torque switched reluctance motors: Teethed-pole and PM-inserted structures, 2020 11th Power Electronics, In: Drive Systems, and Technologies Conference (PEDSTC), Tehran, pp 1–6. <https://doi.org/10.1109/PEDSTC49159.2020.9088418>
- Villalba-Alumberos G, Moron-Alguacil C, Fernandez-Munoz M, Valiente-Blanco I, Diez-Jimenez E (2022) Scale effects on performance of BLDC micromotors for internal biomedical applications: a finite element analysis. *J Med Device* 16:1–10. <https://doi.org/10.1115/1.4054495>
- Ji T-H, Kim C-H, Yoon H-J, Kim Y-J, Jung S-Y (2021) Power density improvement of FSCW axial flux permanent magnet motors by designing shape of back yoke. In: 2021 24th International Conference on Electrical Machines and Systems (ICEMS), Gyeongju, pp 1274–1278. <https://doi.org/10.23919/ICEMS52562.2021.9634377>

4. Ghodsi M, Ueno T, Higuchi T (2008) Novel magnetostrictive bimetal actuator using permendur. *Adv Mater Res* 47–50(PART 1):262–265. <https://doi.org/10.4028/www.scientific.net/AMR.47-50.262>
5. You D, Jang S, Lee J, Sung T (2008) Dynamic performance estimation of high-power FESS using the operating torque of a PM synchronous motor / generator 44:4155–4158. <https://doi.org/10.1109/TMAG.2008.2002607>
6. He X, Guo H, Ding X, Tian W (2019) Design of High-Power and High-Speed PM Assisted Synchronous Reluctance Aero-Starter-Generator, 2019 22nd International Conference on Electrical Machines and Systems (ICEMS). Harbin, China, pp 1–5. <https://doi.org/10.1109/ICEMS.2019.8922269>
7. Yin H, Yu Y, Li J (2017) Optimization design of a motor embedded in a lightweight robotic joint. In: 2017 12th IEEE Conference on Industrial Electronics and Applications (ICIEA), Siem Reap, pp 1630–1634. <https://doi.org/10.1109/ICIEA.2017.8283100>
8. Perez-Diaz JL, Diez-Jimenez E, Valiente-Blanco I, Cristache C, Alvarez-Valenzuela M-A, Sanchez-Garcia-Casarrubios J et al (2015) Performance of magnetic-superconductor non-contact harmonic drive for cryogenic space applications. *Machines* 3:138–156. <https://doi.org/10.3390/machines3030138>
9. Cristache C, Diez-Jimenez E, Valiente-Blanco I, Sanchez-Garcia-Casarrubios J, Perez-Diaz J-L (2016) Aeronautical magnetic torque limiter for passive protection against overloads. *Machines* 4(3):17. <https://doi.org/10.3390/machines4030017>
10. Koser H, Lang JH (2006) Magnetic induction micromachine - Part I: Design and analysis. *J Microelectromech Syst* 15:415–426. <https://doi.org/10.1109/JMEMS.2006.872238>
11. Esnoz-Larraya J, Valiente-Blanco I, Cristache C, Sanchez J, Rodriguez-Celis F, Diez-Jimenez E et al (2017) OPTIMAGDRIVE: high performance magnetic gears development for space applications. In: European Space Mechanisms and Tribology Symposium Tribol (ESMATs). University of Hertfordshire, Hatfield, pp 1–5
12. Diez-Jimenez E, Sanchez-Montero R, Martinez-Muñoz M (2017) Towards miniaturization of magnetic gears: torque performance assessment. *Micromachines* 9:16. <https://doi.org/10.3390/mi9010016>
13. Baschiroto A, Dallago E, Malcovati P, Marchesi M, Melissano E, Siciliano P et al (2006) An integrated micro-fluxgate magnetic sensor with sputtered ferromagnetic core. In: IEEE instrumentation and measurement technology conference proceedings, vol 2006, Sorrento, pp 2045–2049. <https://doi.org/10.1109/IMTC.2006.328426>
14. Iijima Y, Houjou Y, Sato R (2000) Millimeter wave absorber using M-type hexagonal ferrite. In: IEEE international symposium on electromagnetic compatibility, vol 2, Washington, pp 547–549. <https://doi.org/10.1109/ISEMC.2000.874679>
15. Diez-Jimenez E, Valiente-Blanco I, Perez-Diaz J (2012) Superconducting sphere and finite-size permanent magnet: force, torque, and alignment effect calculation. *J Supercond Nov Magn* 26:71–75. <https://doi.org/10.1007/s10948-012-1707-x>
16. Perez-Diaz JL, Diez-Jimenez E, Valiente-Blanco I, Cristache C, Alvarez-Valenzuela M-A, Sanchez-Garcia-Casarrubios J (2014) Contactless mechanical components: gears, torque limiters and bearings. *Machines* 2(4):312–324. <https://doi.org/10.3390/machines2040312>
17. Serrano-tellez J, Romera-juarez F, González-de-maría D, Lamensans M, Perez-Diaz JL, Sanchez-Casarrubios J et al (2012) Experience on a cryogenic linear mechanism based on superconducting levitation. In: Modern technologies in space- and ground-based telescopes and instrumentation II, vol 8450. Proceedings of the SPIE. <https://doi.org/10.1117/12.925165>
18. Chah A, Belharet K, Hei J (2022) Soft ferromagnetic microrobot navigation in the cochlea using haptic assistance. In: IEEE/ASME International Conference on Advanced Intelligent Mechatronics (AIM), vol 2022, Sapporo, pp 626–631. <https://doi.org/10.1109/AIM52237.2022.9863291>
19. Lee FC, Fellow L, Li Q (2013) High-frequency integrated point-of-load converters: overview. *IEEE* 28:4127–4136. <https://doi.org/10.1109/TPEL.2013.2238954>
20. Alderman AN, Panossian V (2008) PSMA marketing and technology report: power supply in a package, power supply on a chip. Power Sources Manufacturers Association [online available]: <http://pwrsocevents.com/wp-content/uploads/2008-presentations/Invited%20Talk%20S6x5%20-%20Arnold%20Alderman%20-%20Update%20on%20PSMA%20Study%20of%20Power%20Supply%20in%20Package%20Vs%20Power%20Supply%20on%20Chip.pdf>
21. Foley R, Waldron F, Slowey J, Alderman A, Narveson B, O'Mathúna SC (2010) Technology roadmapping for Power Supply in Package (PSiP) and Power Supply on Chip (PwrSoC). In: Twenty-fifth annual IEEE Applied Power Electronics Conference and Exposition (APEC). Palm Springs, CA, pp 525–532. <https://doi.org/10.1109/APEC.2010.5433622>
22. Dinulovic D, Shousha M, Haug M, Gerfer A, Beringer S, Wurz MC et al (2019) Microfabricated magnetics on silicon for point of load high-frequency DC–DC converter applications. *IEEE* 55:5068–5077. <https://doi.org/10.1109/TIA.2019.2921523>
23. Dinulovic D, Kaiser M, Gerfer A, Opitz O, Wurz MC, Rissing L et al (2014) Applications microtransformer with closed Fe-Co magnetic core for high frequency power applications. *J Appl Phys* 115:17A317. <https://doi.org/10.1063/1.4863930>
24. Diez-jimenez E, Valiente-blanco I, Villalba-alumbrosos G, Fernandez-munoz M, Lopez-pascual D, Lastra-sedano A et al (2022) Multilayered microcoils for microactuators and characterization of their operational limits in body-like environments. *IEEE/ASME Trans Mechatron*. <https://doi.org/10.1109/TMECH.2022.3215233>
25. Sullivan CR, Member S, Harburg DV, Member S, Qiu J, Member S et al (2013) Integrating magnetics for on-chip power: a perspective. *IEEE* 28:4342–4353. <https://doi.org/10.1109/TPEL.2013.2240465>
26. Ouyang Z, Andersen MAE (2014) Overview of planar magnetic technology — fundamental properties. *IEEE* 29:4888–4900. <https://doi.org/10.1109/TPEL.2013.2283263>
27. Khan F, Zhu Y, Lu J, Pal J, Dao DV (2015) Micromachined coreless single-layer transformer without crossovers. *IEEE* 6:5–8. <https://doi.org/10.1109/LMAG.2015.2477480>
28. Sundar RS, Deevi SC (2005) Soft magnetic FeCo alloys: alloy development, processing, and properties. *Int Mater Rev* 50:157–192. <https://doi.org/10.1179/174328005x14339>
29. Pramanik S, Andreiev A, Hoyer KP, Schaper M (2021) Quasi in-situ analysis of fracture path during cyclic loading of double-edged U notched additively manufactured FeCo alloy. *Int J Fatigue* 153:106498. <https://doi.org/10.1016/j.ijfatigue.2021.106498>
30. Zhou B, Yang Y, Qin Y, Yang G, Wu M (2022) Fabrication of equiatomic FeCo alloy parts with high magnetic properties by fields activated sintering. *Manuf Rev* 9:7. <https://doi.org/10.1051/mfreview/2022001>
31. Silveyra JM, Ferrara E, Huber DL, Monson TC (2018) Soft magnetic materials for a sustainable and electrified world. *Science* 362:1–9. <https://doi.org/10.1126/science.aao0195>
32. Torres MB, Aguado A, Aguilera-Granja F, Vega A, Balbás LC (2015) Structural, vibrational, and magnetic properties of FeCoOn0/+ (n = 1–6) bimetallic oxide clusters. *J Phys Chem C* 119:11200–11209. <https://doi.org/10.1021/JP5121349>
33. Munoz F, Alici G, Li W, Sitti M (2016) Size optimization of a magnetic system for drug delivery with capsule robots. *IEEE Trans Magn* 52(5):1–11. <https://doi.org/10.1109/TMAG.2016.2519004>
34. Kazakova MA, Koul A, Golubtsov GV, Selyutin AG, Ishchenko AV, Kvon RI et al (2021) Nitrogen and oxygen functionalization of multi-walled carbon nanotubes for tuning the bifunctional oxygen reduction/oxygen evolution performance of supported FeCo

- oxide nanoparticles. *ChemElectroChem* 8:2803–2816. <https://doi.org/10.1002/celec.202100556>
35. Pflieger W, Glunz SW (2000) Laser micromachining for applications in thin film technology. *Appl Surf Sci* 154–155:633–639. [https://doi.org/10.1016/S0169-4332\(99\)00468-7](https://doi.org/10.1016/S0169-4332(99)00468-7)
  36. Xu Y, Yao B, Wang E, Fan Y, Lou B, Guo Y (2021) Fabrication of FeCo and CoFe<sub>2</sub>O<sub>4</sub> nanowire arrays and magnetic properties. *Phys E Low-Dimens Syst Nanostruct* 130:114695. <https://doi.org/10.1016/j.physe.2021.114695>
  37. Li FS, Zhou D, Wang T, Wang Y, Song LJ, Xu CT (2007) Fabrication and magnetic properties of FeCo alloy nanotube array. *J Appl Phys* 101:1–4. <https://doi.org/10.1063/1.2405729>
  38. Mostaan H, Shamanian M, Safari M (2016) Process analysis and optimization for fracture stress of electron beam welded ultra-thin FeCo-V foils. *Int J Adv Manufact Technol* 87:1045–1056. <https://doi.org/10.1007/s00170-016-8553-0>
  39. Chang TW, Liao KW, Lin CC, Tsai MC, Cheng CW (2021) Predicting magnetic characteristics of additive manufactured soft magnetic composites by machine learning. *Int J Adv Manufact Technol* 114:3177–3184. <https://doi.org/10.1007/s00170-021-07037-y>
  40. Silva A, Lozano JA, Machado R, Escobar JA, Wendhausen PAP (2008) Study of soft magnetic iron cobalt based alloys processed by powder injection molding. *J Magn Magn Mater* 320:393–396. <https://doi.org/10.1016/j.jmmm.2008.02.178>
  41. Deng D, Wan W, Huang Q, Huang X, Zhou W (2016) Investigations on laser micromilling of circular micro pin fins for heat sink cooling systems. *Int J Adv Manufact Technol* 87:151–164. <https://doi.org/10.1007/s00170-016-8468-9>
  42. Račiukaitis G (2021) Ultra-short pulse lasers for microfabrication: a review. *IEEE J Sel Top Quantum Electron* 27(6):1–12. <https://doi.org/10.1109/JSTQE.2021.3097009>
  43. Singh M, Singh A, Ramkumar J (2019) Thin - wall micromachining of Ti – 6Al – 4V using micro - wire electrical discharge machining process. *J Braz Soc Mech Sci Eng* 41:338. <https://doi.org/10.1007/s40430-019-1827-3>
  44. Cao DM, Jiang J, Yang R, Meng WJ (2006) Fabrication of high-aspect-ratio microscale mold inserts by parallel  $\mu$ EDM. *Microsyst Technol* 12(9):839–845. <https://doi.org/10.1007/s00542-006-0131-1>
  45. Chen N, Li HN, Wu J, Li Z, Li L, Liu G et al (2021) Advances in micro milling: from tool fabrication to process outcomes. *Int J Mach Tools Manuf* 160:103670. <https://doi.org/10.1016/j.ijmactools.2020.103670>
  46. O'Toole L, Kang CW, Fang FZ (2021) Precision micro-milling process : State of the art. *Adv Manuf* 9(2):173–205. <https://doi.org/10.1007/s40436-020-00323-0>
  47. Cheng K, Huo D (2013) *Micro-cutting: fundamentals and applications*. John Wiley & Sons, Ltd, Chichester, United Kingdom
  48. Li Y, Cheng X, Ling S, Zheng G, He L (2022) Study on deformation and compensation for micromilling of thin walls. *Int J Adv Manuf Technol* 120:2537–2546. <https://doi.org/10.1007/s00170-022-08798-w>
  49. CrichignoFilho JM, Melotti S (2022) Evaluation of an experimental modal analysis device for micromilling tools. *Int J Adv Manuf Technol* 119:6679–6692. <https://doi.org/10.21203/rs.3.rs-736522/v1>
  50. Gomes MC, da Silva MB, Duarte MAV (2020) Experimental study of micromilling operation of stainless steel. *Int J Adv Manufact Technol* 111:3123–3139. <https://doi.org/10.1016/j.cirpj.2014.10.003>
  51. Serje D, Pacheco J, Diez E (2020) Micromilling research: current trends and future prospects. *Int J Adv Manufact Technol* 111:1889–1916. <https://doi.org/10.1007/s00170-020-06205-w>
  52. Wan M, Wen DY, Ma YC, Zhang WH (2019) On material separation and cutting force prediction in micro milling through involving the effect of dead metal zone. *Int J Mach Tools Manuf* 146:103452. <https://doi.org/10.1016/j.ijmactools.2019.103452>
  53. Ding H, Ibrahim R, Cheng K, Chen SJ (2010) Experimental study on machinability improvement of hardened tool steel using two dimensional vibration-assisted micro-end-milling. *Int J Mach Tools Manuf* 50:1115–1118. <https://doi.org/10.1016/j.ijmactools.2010.08.010>
  54. Balázs BZ, Geier N, Takács M, Davim JP (2021) A review on micro-milling: recent advances and future trends. *Int J Adv Manufact Technol* 112:655–684. <https://doi.org/10.1007/s00170-020-06445-w>
  55. Kawahara K (1983) Effect of additive elements on cold workability in FeCo alloys. *J Mater Sci* 18:1709–1718. <https://doi.org/10.1007/BF00542066>
  56. Nabi B, Helbert AL, Brisset F, André G, Waeckerlé T, Baudin T (2013) Effect of recrystallization and degree of order on the magnetic and mechanical properties of soft magnetic FeCo-2V alloy. *Mater Sci Eng A* 578:215–221. <https://doi.org/10.1016/j.msea.2013.04.066>

**Publisher's note** Springer Nature remains neutral with regard to jurisdictional claims in published maps and institutional affiliations.